SPARC-BD-03/006
SPARC-RF-03/003
25 November 2003

LONGITUDINAL AND TRANSVERSE PHASE SPACE CHARACTERIZATION

D. Alesini, C. Vaccarezza, *(INFN/LNF)*

Abstract

The characterization of the longitudinal and transverse phase space of the beam provided by the SPARC photoinjector is a crucial point to establish the performance quality of the photoinjector itself. By means of an RF deflector and a dispersive system, the six dimensional beam phase space can be analyzed. In this paper we present the principle and the simulation results of the measurements, together with a detailed description of the RF deflector design.

1 INTRODUCTION

The characterization of the longitudinal and transverse phase space of the beam is a powerful tool in order to verify and tune the photoinjector performance. With the use of an RF deflector it is possible to measure the bunch length [1,2]; adding a dispersive system the longitudinal beam phase space can be completely reconstructed. The longitudinal beam distribution can be projected along a given transverse coordinate at a detector flag and, using the orthogonal transverse coordinate distribution, both the horizontal and vertical beam emittances can be measured with the quadrupole scan technique. A schematic layout of the measurement is reported in Fig.1.

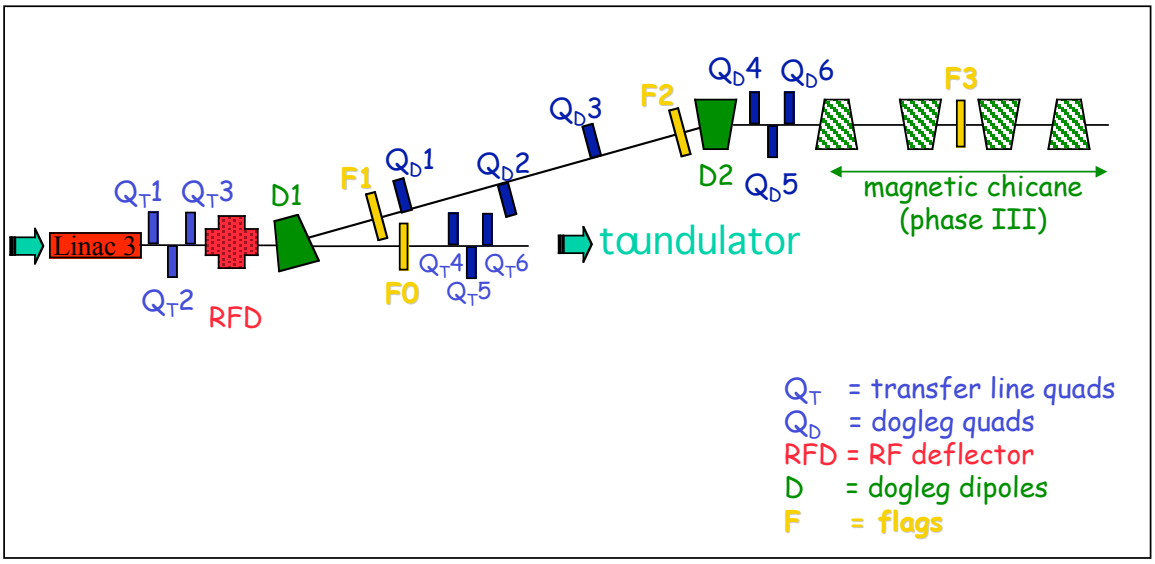

FIG. 1: SPARC measurement layout for high energy beam characterization

In Fig. 2 the effect of the RF deflector is illustrated: the RF deflector voltage (the integrated transverse kick) is null in the longitudinal center of the bunch and gives a linear transverse deflection to the bunch itself. If we consider the beam distribution and a drift space of length L after the deflector, the transverse kick results in a transverse displacement of the centroid of the bunch slice. This displacement is proportional to the slice longitudinal offset L_B, and RF voltage according to the expression

$$x_B = \frac{\square f_{RF} L L_B V_\square}{cE/e} \tag{1}$$

where f_{RF} is the frequency of the deflecting voltage, $V_\square$ is the peak transverse voltage, and E/e is the beam energy in eV units. More complicated expressions result when one considers magnetic components instead of a simple drift space between the deflector and detector. Equation (1) shows that the longitudinal bunch distribution can be obtained by measuring the transverse bunch distribution at the position z_s.

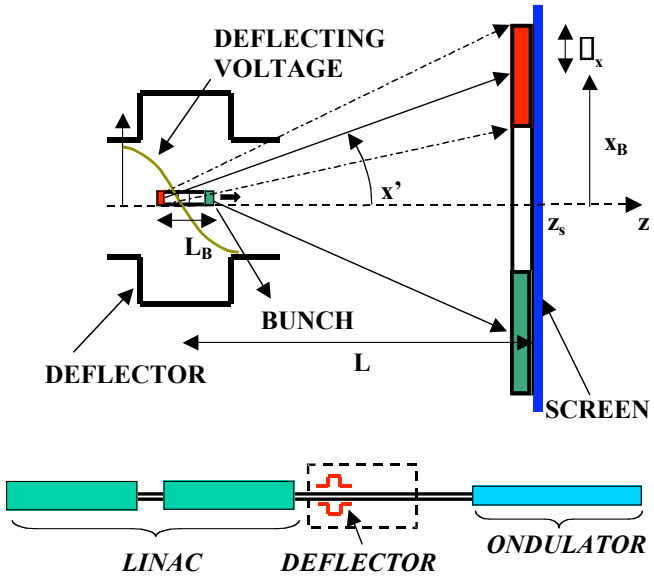

FIG. 2: Bunch length measurement schematic setup using an RF deflector.

As illustrated in Fig. 2 the transverse distribution of the bunch at the position z_s is the convolution between the displaced slices and the proper transverse slice sizes at the position z_s. In order to measure the bunch length with the proper accuracy, the displaced position x_B has to be bigger than σ_x. The resolution length (L_{res}) can be defined, therefore, as the relative slice longitudinal position that gives, on the screen, an x_B equal to σ_x. By use of Eq. (1) we can calculate the transverse voltage $V_\perp$ necessary to achieve a certain resolution:

$$V_\perp = \frac{\sigma_x cE/e}{2\pi f_{RF} L L_{res}} \tag{2}$$

A sketch of the complete longitudinal phase space measurement setup is shown in Fig. 3. In this scenario, the bunch is vertically deflected by the RF deflector and horizontally by a magnetic dipole. The dispersion properties of the dipole allow to completely characterize the energy distribution of the bunch and the total longitudinal phase space can be displayed on the screen.

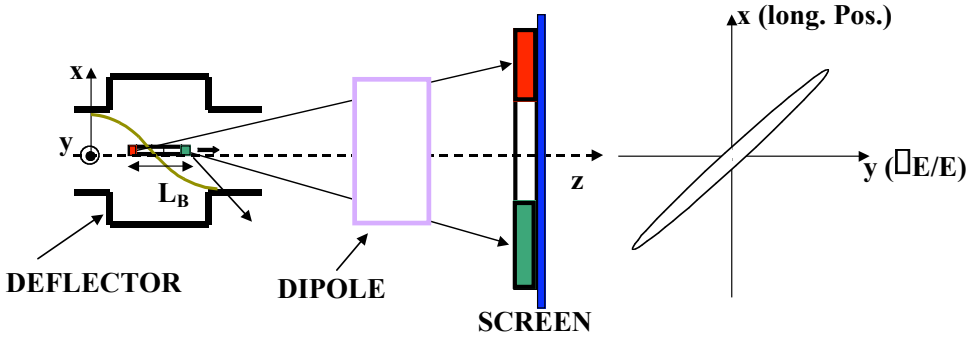

FIG. 3: Longitudinal phase space measurement setup using an RF deflector and a dipole magnet.

The transverse phase space characterization is obtained measuring the beam slice emittance in both the transverse planes. The slice emittance is the transverse emittance of a short time interval (slice) of the microbunch. It can be measured using a beam with a linear energy-time correlation, or chirp; the chirp is combined with the quadrupole scan technique to determine the emittance of the slices along the bunch [3-5]. This type of energy-time correlation can be provided by the RF deflector or by use of the dispersive system.

Using the RF deflector the horizontal slice emittance ε_x can be measured either on the transfer lines or on the dogleg, at the flags F0 and F3, respectively. The beam emittance can be calculated by the following expression:

$$\sigma_{11}\sigma_{22} - \sigma_{12}^2 = \varepsilon^2 \tag{3}$$

where the measured quantities σ_{11}, σ_{21} and σ_{22} are the second moments of the horizontal trace space. This relationship is indicated in compact form through the equation of an n-dimensional ellipse written as

$$\mathbf{u}^T \Sigma^{-1} \mathbf{u} = 1 \tag{4}$$

where $\mathbf{u}$ and $\mathbf{u}^T$ are the coordinate vector and its transpose, and Σ is a symmetric matrix.The first two quads after the linac sections, Q_T1 and Q_T2 , are used in this case for the quadrupole scan: the beam horizontal size at the the screen (F0,F3) is varied keeping constant the vertical one. The measurement results are fitted following the equation

$$\sigma_{11}^{screen} = R_{11}^2 \sigma_{11}^{s_o} + 2R_{12}R_{11}\sigma_{12}^{s_o} + R_{12}^2 \sigma_{22}^{s_o} \tag{5}$$

where σ_{11}^{screen} is the horizontal beam rms size measured at the screen , and R_{11} and R_{12} are the first two elements of the matrix governing the beam transport from the first scanning quadrupole to the screen considered.

With the dispersive system the same two quads are used to vary the vertical beam size at the location of the flag F2 with an opportune value of the horizontal dispersion. The third linac section is dephased of about 30° to produce the desired energy chirp. The measured values of the rms vertical beam size are fitted to obtain the vertical beam slice emittance.

2 SIMULATIONS RESULTS

2.1 Longitudinal phase space measurement

Using Eqs. (1) and (2) it is possible to calculate the total transverse dimensions of the bunch as a function of the deflecting voltage $V_\perp$ and needed deflecting voltage $V_\perp$ as a function of

L_{res}. The results are plotted in Figs. 4(a) and 4(b), assuming L_B=4 mm, E/e=150 MV, L=2 m and $\sigma_x = 30\mu m$.

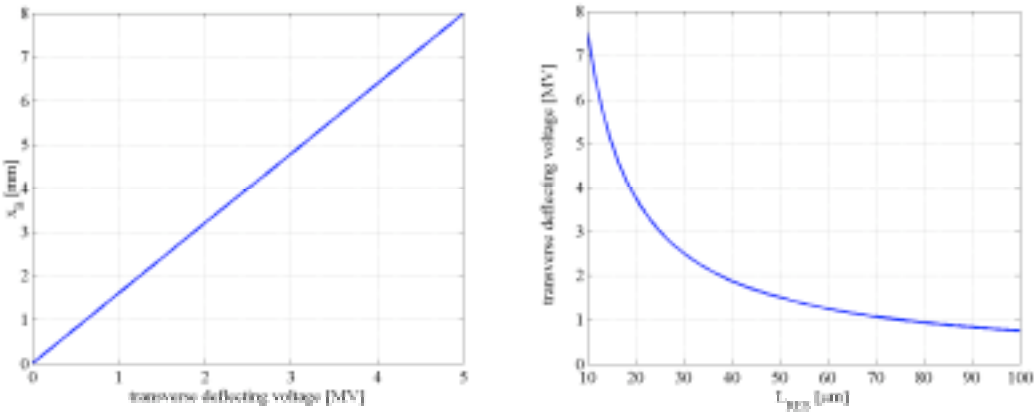

FIG. 4: (a) total transverse dimensions of the bunch as a function of the deflecting voltage $V_\perp$; (b) deflecting voltage $V_\perp$ as a function of L_{res}.

From these considerations, as well as a desire to mitigate the total power needed, a voltage $V_\perp$=1.0 MV has been chosen for the RF deflector. A 150k particle beam obtained from PARMELA simulation at the end of the linac section has been tracked with the ELEGANT code along the SPARC transfer lines. The images of the beam obtained at the RF deflector location and at the screen location, F0, are shown in Figs. 5 and 6.

The results of the data analysis are shown in Fig 7 where the vertical projected and the longitudinal distributions of the bunch are displayed. The value of σ_z as obtained by applying Eq. (1) and by the longitudinal analysis of the raw data obtained from ELEGANT tracking agree with an error less than 1%.

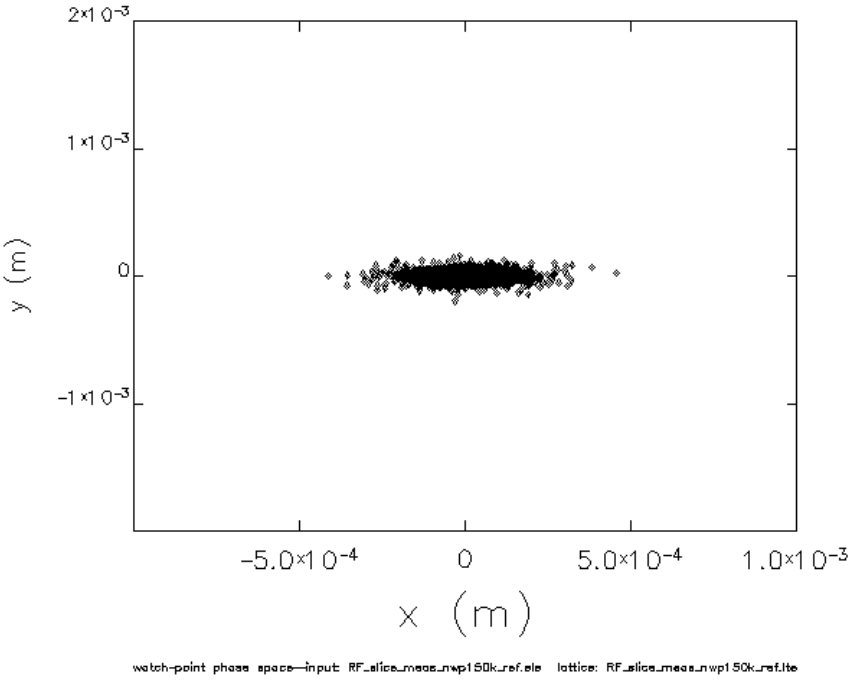

FIG. 5: Bunch transverse distribution at the RF deflector location.

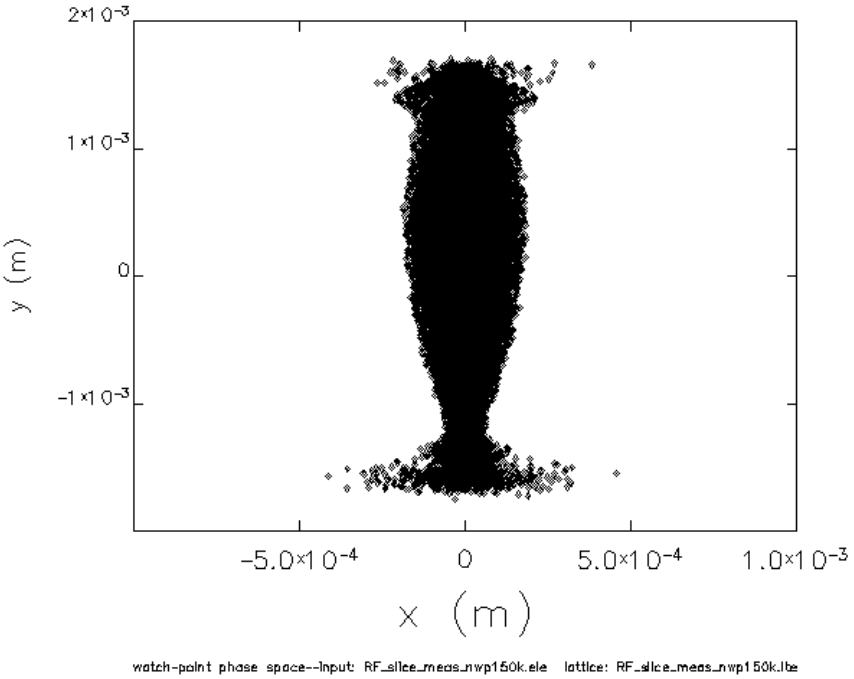

FIG. 6: Bunch transverse distribution at the RF deflector location.

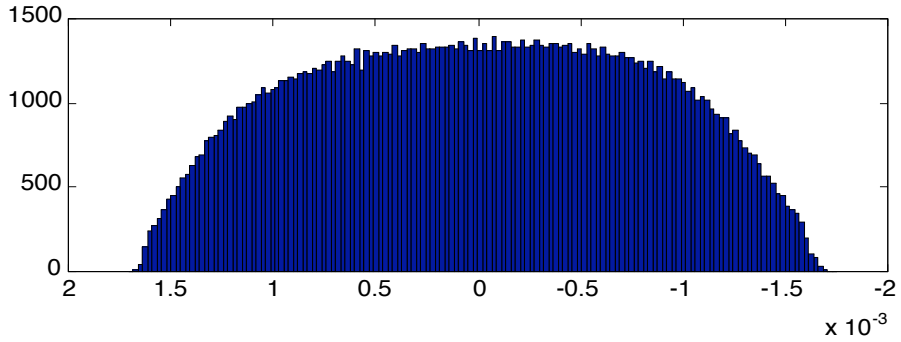

FIG. 7: Above: the longitudinal bunch distribution as projected by the RF deflector on the vertical coordinate of the screen F0; below: the same bunch longitudinal distribution vs. time.

The images collected on the dogleg at the screen located in F1 show the complete reconstruction of the longitudinal phase space as shown in Figs. 8 and 9 where the time-energy (*t,p*) distribution is replicated in the transverse plane (*y,x*). The "reconstructed" rms energy spread value is in very good agreement with the real one. The slice analysis is under study to take into account all the relevant effects.

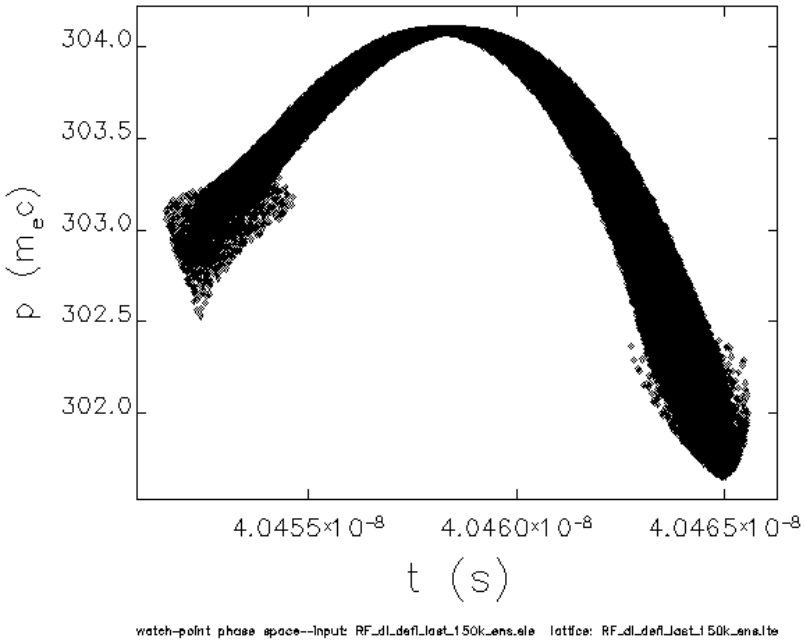

FIG. 8: Bunch longitudinal distribution vs time at F1.

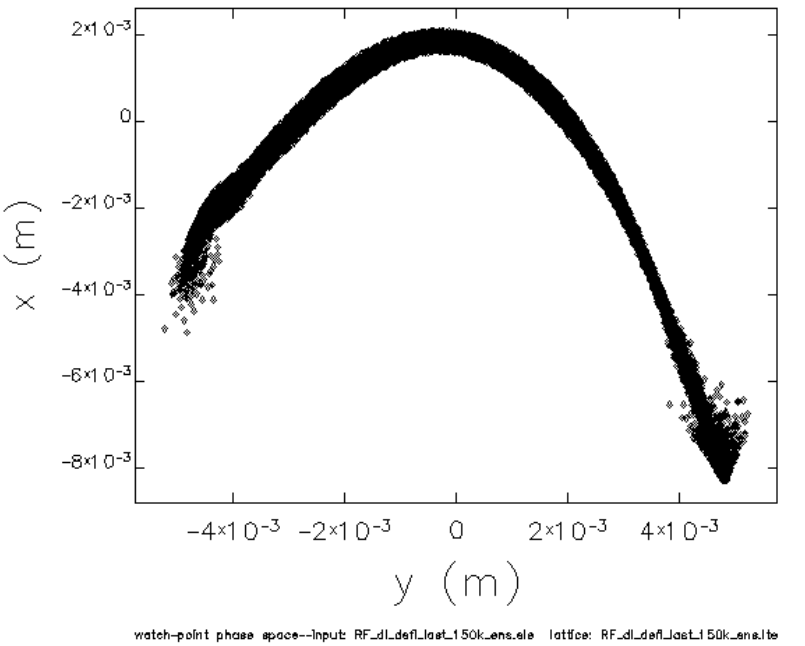

FIG. 9: Bunch transverse distribution at F1

2.2 Transverse phase space

To measure the beam slice emittance in the horizontal plane the RF deflector can be used scanning the beam rms size at the screen locations F0 and F3, where two different values of image resolution can be achieved for the minimum horizontal rms size reconstruction. For the vertical emittance the dispersive system can be used with the beam image being examined at the screen location F2. In Figs. 10 and 11 the optic functions of the SPARC transfer lines and dogleg are reported for the measurement setup of the horizontal emittance.

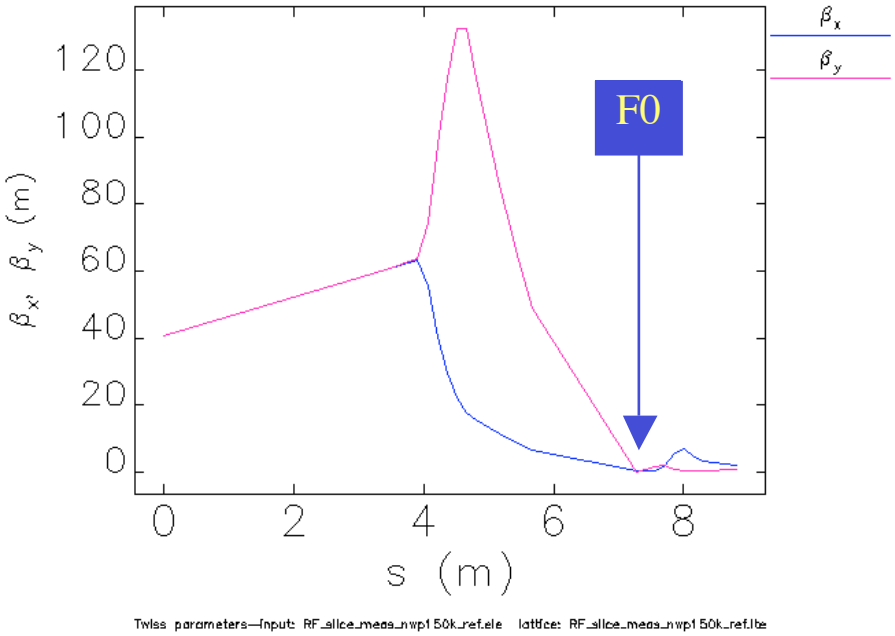

FIG. 10: SPARC transfer lines optic functions for the horizontal quad scan at F0. The origin of the longitudinal coordinate corresponds to the exit of the second linac section.

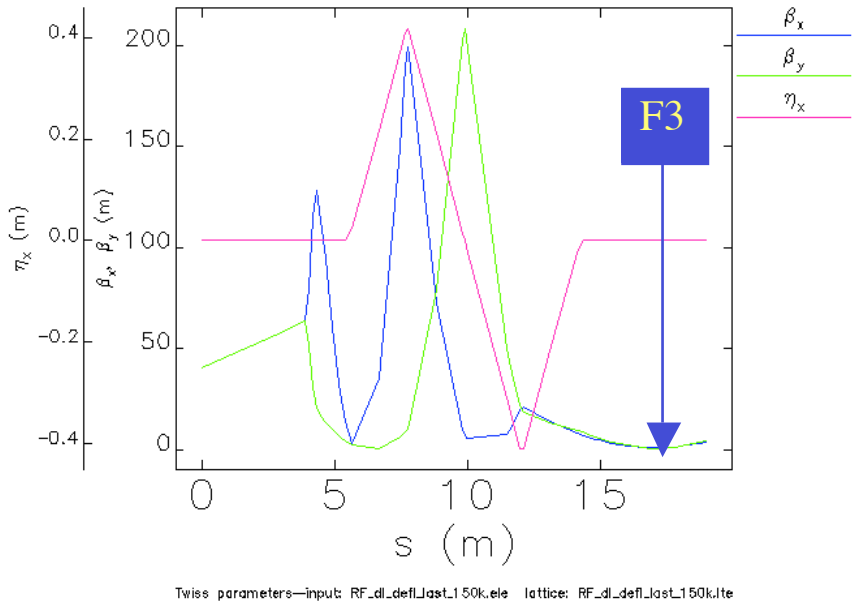

FIG. 11: SPARC dogleg optic functions for the horizontal quad scan at F3. The origin of the longitudinal coordinate corresponds to the exit of the second linac section.

In Fig. 12 the beam horizontal slice emittance is given for the two simulated measurements at F0 (left) and F3 (right), respectively. For the top figures, the result of the temporal analysis of the raw data is reported for the two cases; those below show the reconstructed horizontal slice emittance. The main difference between the results obtained scanning at F0 or F3 is the minum value of the rms beam size as can be seen in Fig. 13, where the curves refer to the new SPARC working point optimization (1.1 nC). This aspect provides a tool to investigate a wide range of beam emittance values without loosing the measurement accuracy.

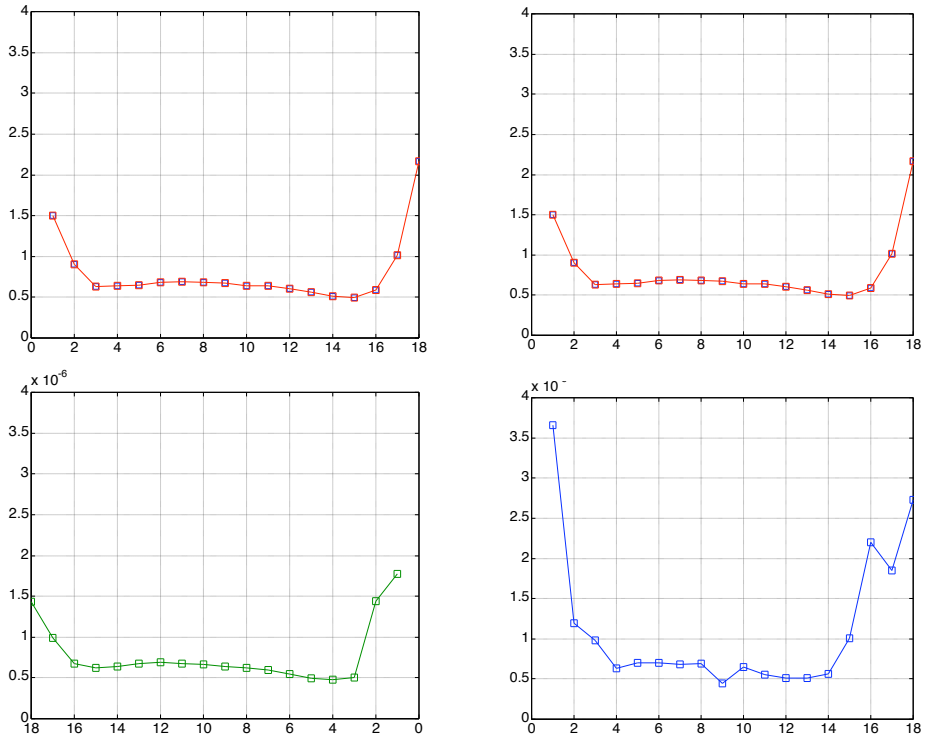

FIG. 12:: Reconstructed horizontal beam slice emittance (in mm-mrad) as a function of slice number with the beam size scanning at F0 (left), and at F3 (right). The a) curves (above) is the horizontal emittance as calculated by slicing the beam along the temporal coordinate, the b) curves (below) are the result of the two quadrupole scan at the two screen locations.

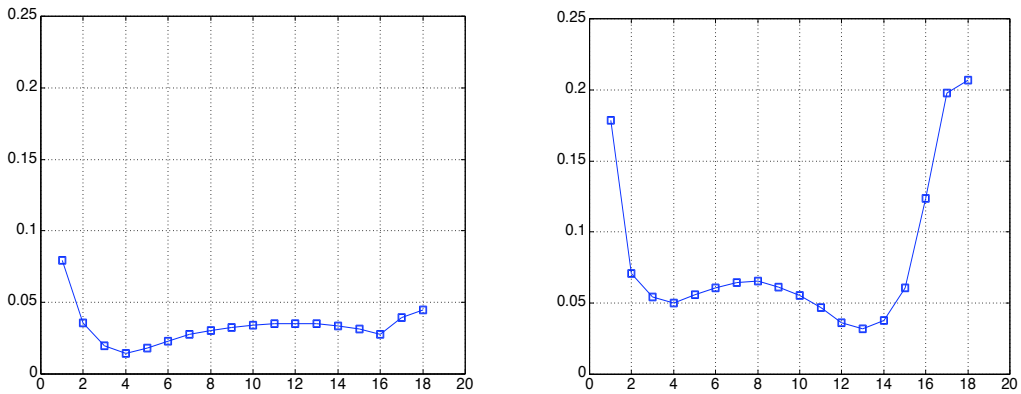

FIG. 13: Minimum horizontal rms beam size (cm) at the two screen locations: F0 (left), and F3 (right) during the quadrupole scan.

3 RF DEFLECTOR DESIGN

The simplest and more efficient multi-cell deflecting structure that can be used to deflect the bunch is a standing wave structure operating in the π-MODE. In Fig. 14 it is shown, as an example, a simple 5-cells cavity with beam pipe tubes. The external radius (b) has been chosen in order to tune the resonant frequency of the π-MODE to 2.856 GHz, the internal radius (a) is equal to the beam pipe radius (20 mm), the cell length (d) is equal to $c/2f_{RF}$ to synchronize the bunch passage and the deflecting field. The iris thickness (t) has been chosen as a reasonable value of 9.5 mm, considering that it is not a critical dimension in term of sensitivities.
The dispersion curves of the single cell as obtained by MAFIA 2D [6] simulations with b=60 mm are reported in Fig. 15. The deflecting π-MODE has a frequency equal to 2.856 GHz, while the nearest monopole and dipole modes are far away from the deflecting mode.
The deflecting voltage $V_\perp$ is related to the dissipated power in the cavity P_{RF} (equal to the input power if the coupling coefficient between the generator and the cavity is equal to 1) and the transverse shunt impedance $R_\perp$ by the relation:

$$V_\perp = \sqrt{2 P_{RF} R_\perp} \tag{6}$$

The total transverse shunt impedance $R_\perp$, quality factor Q, and frequency separation with respect to the nearest modes Δf, as a function of the number of cells n, has been calculated by MAFIA 2D. The results of this study are reported in Table 1. The transverse shunt impedance scales approximately as $R_\perp \cong 0.5 M\Omega * n$ while the quality factor is practically independent of n.
The peak surface electric field E_P in the structure has been found to scale approximately as:

$$E_P \left[\frac{MV}{m}\right] \cong 90 \sqrt{\frac{P_{RF}[MW]}{n}} \tag{7}$$

Therefore with an input power P_{RF}=2 MW we obtain $E_P \cong 60$ MV/m with 5 cells and a marginally unacceptable $E_p \cong 130$ MV/m with 1 cell.
The previous results allow us to choose the number of cells for the deflecting structure. The choice can be optimized considering the following considerations:

a) the available transverse deflecting voltage for a given input power;
b) the available space in the SPARC transfer line;
c) the mode separation with different number of cells to avoid problems of mode overlapping;
d) the maximum acceptable surface peak electric field to avoid problems related to high field intensities, discharges and so on.

The 5-cell deflecting structure fulfills all of the stated requirements. In fact, it allows to operate with a very low input power $P_{RF} \cong 2$MW obtaining contemporary low peak surface

electric field and resolution length of the order of □25 □m at P_{RF}=2MW. These parameters permit measurement of the longitudinal beam profile with good accuracy, even considering the possibility of longitudinal compression factors of up to 20. Moreover the operation at low input power (□2MW) allows to simplify the power line design as discussed below.

TAB 1: Deflecting cavity properties obtained by MAFIA 2D simulations as a function of the number of cells.

Number of cells	Total length cells [m]	Transverse Impedance [M□]	Quality factor	Bandwith [kHz]	Nearest mode frequency separation [MHz]
3	0.16	1.5	17100	167	25
5	0.26	2.5	16700	171	6
9	0.47	4.5	16900	169	1.5

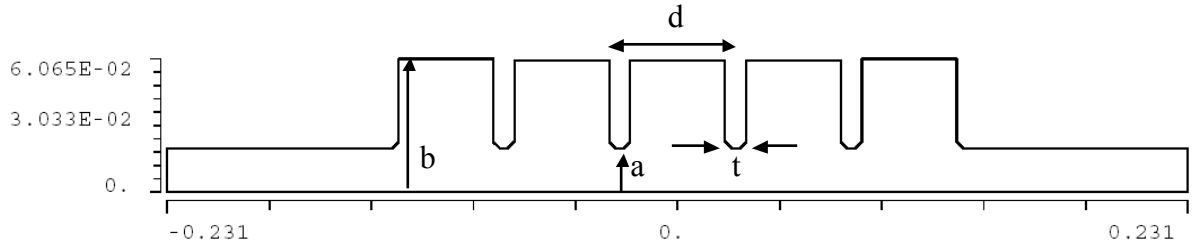

FIG. 14: The transverse profile of the 5-cell deflecting cavity.

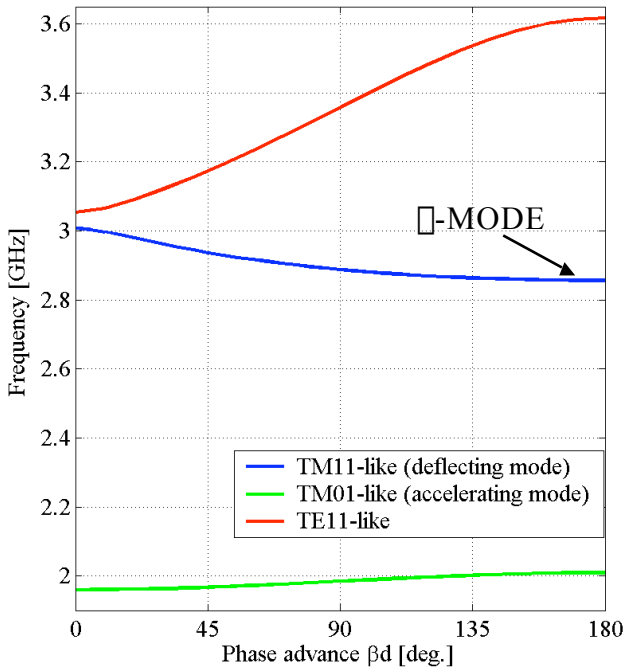

FIG. 15: Single cell dispersion curves of deflection-mode standing wave structures obtained by MAFIA 2D simulations.

3.1 5-cell RF deflector design procedure

3.1.1 2D profile study

The 2D profile of the 5-cell RF deflector has been studied using the MAFIA 2D code. The frequency sensitivities of the single cell profile with respect to the dimensions are reported in Table 2. The simulated 5-cell profile is reported in Fig. 16 with the dimensions shown in Table 3. The radius of the cells connected to the beam pipe tube in this design has been changed in order to achieve a field flatness of 3%. The on-axis magnetic field profile in the structure is plotted in Fig. 17 and the results of the MAFIA simulations in term of resonant frequency, transverse shunt impedance and quality factor are reported in Table 4. These calculated quantities are also compared with the HFSS [7] results discussed in the next paragraph.
To evaluate the sensitivities of the resonant frequency and field flatness as a function of the single cell dimensions, a battery of simulations have been performed. The results are reported in Table 5 and Fig 18 for the most critical parameter *b*. From this study, it is possible to conclude that errors in the cells machining of the order on 10^{-2} mm give frequency errors of the order of 100 kHz and field errors of few percent. These errors can be easily compensated by a proper tuning procedure.

TAB 2: Frequency sensitivities of the single cell profile with respect to the cell dimensions.

Dimension	nominal value [mm]	sensitivity ·[kHz/□m]
a	20.00	-19
b	60.00	-43
t	9.50	1.2
d	52.48	1.8

TAB 3: Dimensions of the 5-cell structure.

Dimension	value [mm]
a	20.00
b2=b3	59.97
b1	60.67
t	9.50
d	52.48

TAB 4: Simulation results of the 5-cells deflecting cavity
(comparison between MAFIA 2D and HFSS)

	MAFIA	HFSS
Frequency [GHz]	2.85699	2.85467
Q	16800	16400
$R_{\square}$ [$M\square$]	2.47	2.43

TAB 5: Resonant frequency sensitivity with respect to the external radius b.

Dimension	sensitivity [kHz/□m]
b1	8.6
b2	10.8
b3	

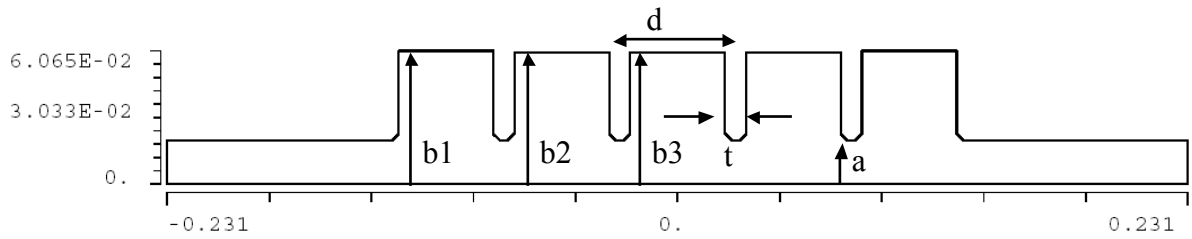

FIG. 16: 5-cells deflecting cavity simulated by MAFIA 2D.

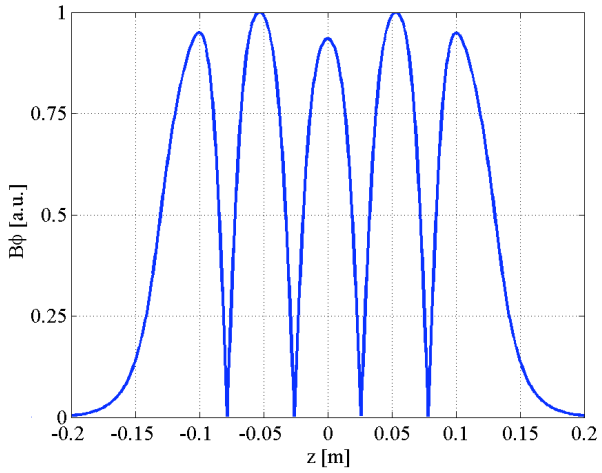

FIG. 17: Absolute value of the magnetic field for the 5-cells cavity obtained by MAFIA 2D simulations.

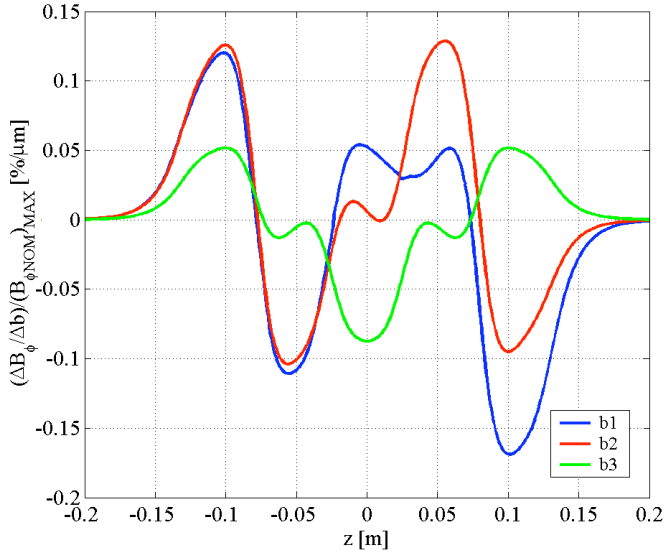

FIG. 18: Relative magnetic field sensitivity with respect to the external radius of the cells.

3.1.2 3D profile study

The 3D simulation study of the deflecting mode structure has been performed using HFSS. The comparison between the 2D and 3D results is shown in Table 4 where we consider the 5-cell structure without coupler.
The coupler design has been chosen to adapt a rectangular waveguide coupler feeding the central cell of the structure. The HFSS simulated structure is plotted in Fig. 19. After some optimization and re-tuning of the central coupler cell we have obtained the result plotted in Figs. 20(a) and (b) in term of field flatness and reflection coefficient at the input port respectively. The obtained coupling factor β and the transverse shunt impedance are equal to 0.94 and 2.11 $M\Omega$, respectively.
A complete investigation has been performed in order to find the mode separation between the desired deflecting mode and the nearest mode within the pass-band. The result is summarized in Table 6. It is important to remark that the nearest modes are not excited by the coupler and can, therefore, perturb only marginally the deflecting field. The nearest mode that can be excited by the coupler is the $\pi/2$ deflecting mode, whose magnetic field profile is shown in Fig. 21.
Concerning the tuning system, the simulations performed on the 3D single cell of Fig. 22 shows that a cylindrical tuning rod of r=5 mm (similar to those found in the RF gun) gives a sensitivity of 550 kHz/mm. This is enough to easily compensate any possible machining error.

TAB. 6: Frequency separation between the deflecting mode and the nearest unwanted modes.

	Excited by the coupler	Δf [MHz]
Deflecting mode tilted polarity (90 deg.)	NO	6.5
$3/4\pi$ mode polarities 0 deg.	NO	5.4
$3/4\pi$ mode polarities 90	NO	5
$\pi/2$ mode	YES	20

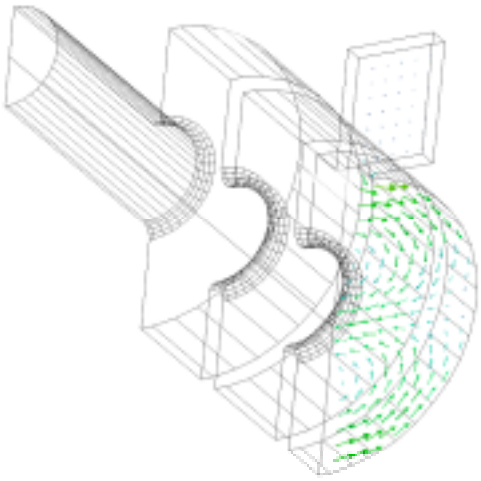

FIG. 19: 3D HFSS simulated structure with coupler.

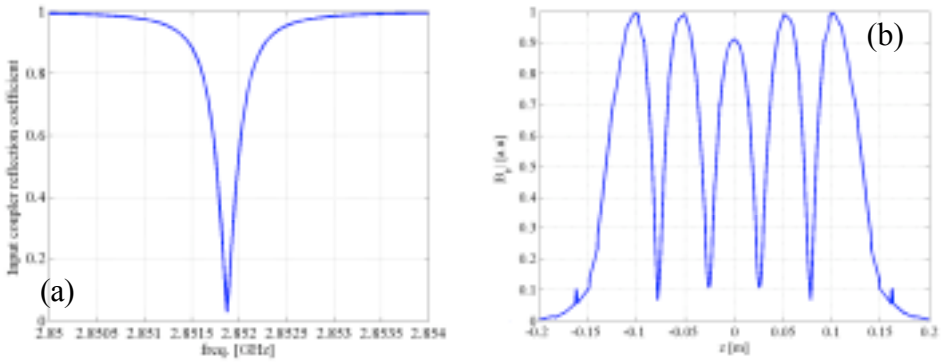

FIG. 20: HFSS coupler simulation results: a) reflection coefficient at the input port; b) on-axis magnetic field profile.

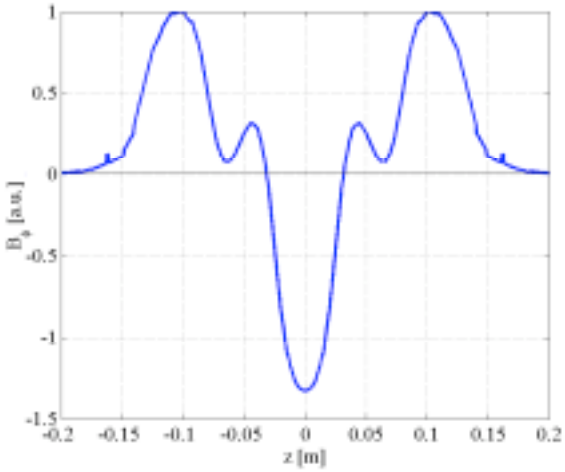

FIG. 21: Magnetic field of the $\pi/2$ deflecting mode excited by the coupler.

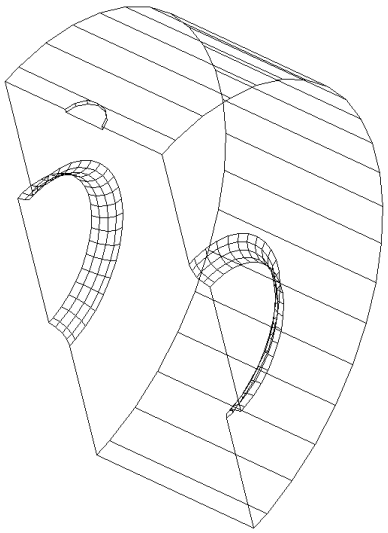

FIG. 22: 3D single cell with tuning system simulated by HFSS.

3.2 RF deflector power feed system

The 2 MW input power needed to feed the structure can be split out from the first klystron waveguide feed with a 10 dB directional coupler, as illustrated in Fig. 23. The circulator and the directional coupler shown assure that every reflected power from the deflector does not interact with the power feeding the RF gun. Moreover the high power switch is included to allow the deflecting field to be completely turned off.
Because of the reduced power needed for the structure it is possible to simply employ a waveguide system with air-fill, thuis reducing the costs of the entire power feed system.

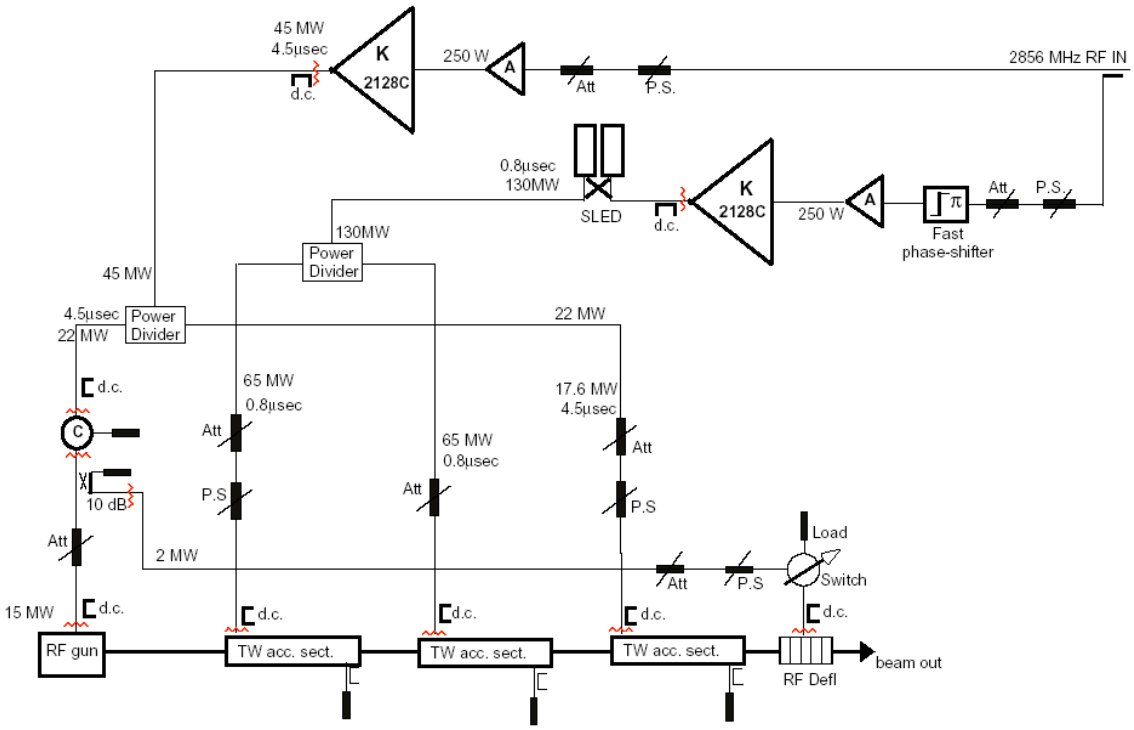

FIG. 23: Sketch of the RF deflector power feed system.

4 CONCLUSIONS

In this paper we have discussed the methods to characterize the longitudinal and transverse phase space at SPARC. They are based on the use of an RF deflector that allows to measure the bunch length or the complete longitudinal phase space by adding a dispersive system. Using the quadrupole scan technique both the horizontal and the vertical beam slice emittances can be measured. The simulations made by the ELEGANT code have shown the feasibility of this diagnostic system.
In the paper we have also discussed the RF deflector design made by the use of the e.m. codes MAFIA and HFSS. It is a 5 cells SW structure working on the π-MODE at 2.856 GHz and feeded by a central coupler with β=1. Since the shunt impedance is $2.5M\Omega$ and the maximum input power is 2 MW, it is possible to obtain a resolution length of the order of $25\mu m$.

5 REFERENCES

[1] P. Emma, et al., “A Transverse RF deflecting structure for bunch length and phase space diagnostics”, LCLS-TN-00-12, 2000.
[2] G.A. Loew, O,H Altenmueller, “Design and applications of RF deflecting structures at SLAC”, PUB-135, Aug. 1965.
[3] D.H. Dowell *et al*, “Slice Emittance Measurements at the SLAC Gun Test Facility”, SLAC-PUB-9540, September 2002
[4] J.F. Schmerge *et al*, “Transverse-emittance measurements on a S-band photocathode RF electron gun”, Nucl. Instr. & Meth. A 483, 2002, pp. 301-304
[5] X. Qiu *et al* ,”Demonstration of Emittance Compensation through the Measurement of the Slice Emittance of a 10- ps Electron bunch”, Phys. Rev. Lett. 76, 20, 1996, pp. 3723-3726.
[6] www.cst.de.
[7] www.ansoft.com.